# The High-frequency Radio Emission of the Galactic Center Magnetar SGR J1745–29 during a Transitional Period

Joseph D. Gelfand[1,2] ⓘ, Scott Ransom[3] ⓘ, Chryssa Kouveliotou[4,5] ⓘ, Jonathan Granot[6] ⓘ, Alexander J. van der Horst[4,5] ⓘ,
Guobao Zhang[1,8,9,10] ⓘ, Ersin GÖĞÜŞ[7] ⓘ, Mallory S. E. Roberts[1] ⓘ, and Hend Al Ali[1] ⓘ

[1] NYU Abu Dhabi, United Arab Emirates
[2] NYU Center for Cosmology and Particle Physics, New York, NY 10003, USA
[3] NRAO, USA
[4] The George Washington University, USA
[5] Astronomy, Physics and Statistics Institute of Sciences (APSIS), Washington, DC 20052, USA
[6] The Open University of Israel, Israel
[7] Sabancı University, Turkey
[8] Yunnan Observatories, Chinese Academy of Sciences, 396 Yangfangwang, Guandu District, Kunming 650216, China
[9] Key Laboratory for the Structure and Evolution of Celestial Objects, Chinese Academy of Sciences, 396 Yangfangwang, Guandu District, Kunming 650216, China
[10] Center for Astronomical Mega-Science, Chinese Academy of Sciences, 20A Datun Road, Chaoyang District, Beijing 100012, China

## Abstract

The origin of the high-frequency radio emission detected from several magnetars is poorly understood. In this paper, we report the $\sim$40 GHz properties of SGR J1745−29 measured using Jansky Very Large Array (JVLA) and Robert C. Byrd Green Bank Telescope (GBT) observations between 2013 October 26 and 2014 May 31. Our analysis of a $Q$-band (45 GHz) GBT observation on 2014 April 10 resulted in the earliest detection of pulsed radio emission at high frequencies ($\gtrsim$20 GHz); we found that the average pulse has a singly peaked profile with width $\sim$75 ms ($\sim$2% of the 3.764 s pulse period) and an average pulsed flux density of $\sim$100 mJy. We also detected very bright, short ($<$10 ms) single pulses during $\sim$70% of this neutron star's rotations, and the peak flux densities of these bright pulses follow the same log-normal distribution as measured at 8.5 GHz. Additionally, our analysis of contemporaneous JVLA observations suggest that its 41/44 GHz flux density varied between $\sim$1–4 mJy during this period, with a $\sim$2$\times$ change observed on $\sim$20 minute timescales during a JVLA observation on 2014 May 10. Such a drastic change over short timescales is inconsistent with the radio emission resulting from a shock powered by the magnetar's supersonic motion through the surrounding medium, but consistent with pulsed emission generated in its magnetosphere.

*Key words:* pulsars: individual (J1745–29) – radio continuum: general – stars: magnetars

## 1. Introduction

Magnetars are believed to be young, isolated neutron stars with extremely strong surface and internal magnetic fields. The resultant stresses are thought to twist the external magnetic field (Thompson et al. 2000), generating persistent currents in the magnetosphere (e.g., Thompson 2008a; Beloborodov 2013). The eventual untwisting of the magnetar's external magnetic field is thought to (e.g., Beloborodov 2009) result in an "activation" event where the source X-ray flux rapidly increases by orders of magnitude, after which it decays over weeks to months to a new quiescent level (e.g., Ibrahim et al. 2004; Mori et al. 2013). Such events have now been observed from about a dozen magnetars, and in a few sources are contemporaneous with the onset of pulsed radio emission (e.g., Camilo et al. 2006, 2007a; Rea et al. 2013), likely a result of the ensuing magnetospheric currents. However, the detection of radio pulsations from a magnetar in X-ray quiescence (Levin et al. 2010) suggests these currents can persist for a long time, though the cessation of radio pulsations does not appear to be connected to the source behavior at X-ray energies (Camilo et al. 2016).

Perhaps not surprisingly, the properties of the pulsed radio emission detected from magnetars are significantly different from those observed from "normal" radio pulsars. Studies of the first radio-emitting magnetar, XTE J1810−197, indicated that its radio pulse profile, pulsed flux density, and pulsed spectrum all varied significantly over timescales as short as a few hours or days (e.g., Camilo et al. 2007b, 2007c). The

detection of a similar behavior (Camilo et al. 2008) from 1E 1547.0−5408 (Camilo et al. 2007a) suggested that such a variability is commonplace among magnetars—in stark contrast to the majority of radio pulsars whose average pulse profile remains constant for years. Additionally, the pulsed $\sim$1–100 GHz radio emission from magnetars typically has a flat (spectral index $\alpha \sim 0$, where flux density $S_\nu \propto \nu^\alpha$) or curved (peak $\nu \sim 10$ GHz) spectrum (e.g., Camilo et al. 2008; Kijak et al. 2013), in sharp contrast with the very steep (average $\alpha \sim -1.6$) spectrum typically observed from most radio pulsars (e.g., Lorimer & Kramer 2012). Furthermore, magnetars emit single, extremely bright and short (few millisecond) long radio pulses far more often than "normal" radio pulsars (e.g., Serylak et al. 2009; Levin et al. 2012). While the origins of these differences—in particular, why the pulsed radio spectrum of magnetars extends to much higher frequencies than that of "normal" radio pulsars—are not yet known, it suggests that the leptons responsible for the pulsed radio emission in magnetars have a different origin and/or acceleration mechanism from those responsible for the pulsed radio emission from "normal" pulsars. It is possible that, in magnetars, these particles are created when X-ray photons emitted from the surface interact with $\gamma$-ray photons generated in the magnetosphere (e.g., Thompson 2008a, 2008b) or are accelerated by currents powered by the untwisting of the magnetic field lines (e.g., Beloborodov 2009, 2013).

SGR J1745−29 was discovered due to a rapid, significant increase in its X-ray flux on 2013 April 24. Analysis of an

observation ∼4–5 days later detected pulsed radio emission (e.g., Rea et al. 2013), whose properties—particularly at high (≳10 GHz) frequencies—have changed considerably since this initial detection. Analysis of Australia Telescope Compact Array observations on 2013 May 1 and 31 indicated that the 16–20 GHz pulsed radio emission of this source had a fairly steep spectrum ($\alpha \sim -2$; Shannon & Johnston 2013), suggesting very faint (<1 mJy) emission at higher frequencies. However, analysis of a Karl G. Jansky Very Large Array (JVLA) observation on 2014 February 21 measured a 41 GHz flux density of $1.62 \pm 0.02$ mJy (Yusef-Zadeh et al. 2014), ∼40× the expected value based on measurements of the pulsed radio spectrum in 2013 May by Shannon & Johnston (2013). This initial detection of SGR J1745−29 at 41 GHz was contemporaneous with significant changes in the 8.5 GHz pulsed flux density and pulse profile (Lynch et al. 2014), possibly suggesting that the appearance of high-frequency radio pulsations is related to its behavior at lower frequencies. Subsequent observations detected pulsed radio emission from this magnetar at frequencies as high as 225 GHz (Torne et al. 2015).

In this paper, we report the results of additional ∼40 GHz observations of this magnetar between 2013 October and 2014 May, the period when high-frequency pulsed radio emission was first detected and the properties of its lower frequency pulsed radio emission changed significantly. In Section 2, we present the results of a 45 GHz Robert C. Byrd Green Bank Telescope (GBT) observation on 2014 April 10, which resulted in the earliest detection of >20 GHz pulsations from this magnetar. In Section 3, we present our analysis of 41/44 GHz JVLA observations between 2013 October 26 and 2014 May 31, during which period we measured significant changes in flux density on both short (∼20 minutes) and long (weeks) timescales. In Section 4, we summarize our results.

## 2. Green Bank Radio Telescope

We observed SGR J1745−29 with the GBT for two hours, starting on 2014 April 10 08:30 (UT), in the Q-band (central frequency of 45 GHz). During this observation, the system temperature was $T_{sys} \approx 80$ K, the zenith opacity was $\tau_{zenith} \approx 0.16$, and the 21°–22° elevation resulted in an airmass $\sec(z) = 2.7$. However, due to instrumental difficulties, we obtained only ∼35 minutes of good data with the Green Bank Ultimate Pulsar Processing Instrument (GUPPI; DuPlain et al. 2008), with an 800 MHz bandwidth, and about ∼30 minutes of good data with the Versatile GBT Astronomical Spectrometer (VEGAS; Bussa & VEGAS Development Team 2012), with a (usable) bandwidth of 5.4 GHz with 1 ms sampling. We present the results of the more sensitive VEGAS data set below; we also searched for pulsations in the less sensitive GUPPI data set but this effort yielded no detection. Unfortunately, VEGAS was not able to record the data needed to measure the polarization of this radio emission. We used the `rednoise` routine (Lazarus et al. 2015) in PRESTO (Ransom 2001) to remove, in the frequency domain, the quasi-periodic oscillations introduced by atmospheric variability.

We then used PRESTO to search for pulsations in the dereddened time series. This analysis indicated statistically significant pulsations with a period $P = 3.763504$ s consistent with previous measurements (period $P \approx 3.764$ s; e.g., Mori et al. 2013), with a singly peaked radio pulse of ∼75 ms duration (considerably longer that the ∼1 ms time resolution of
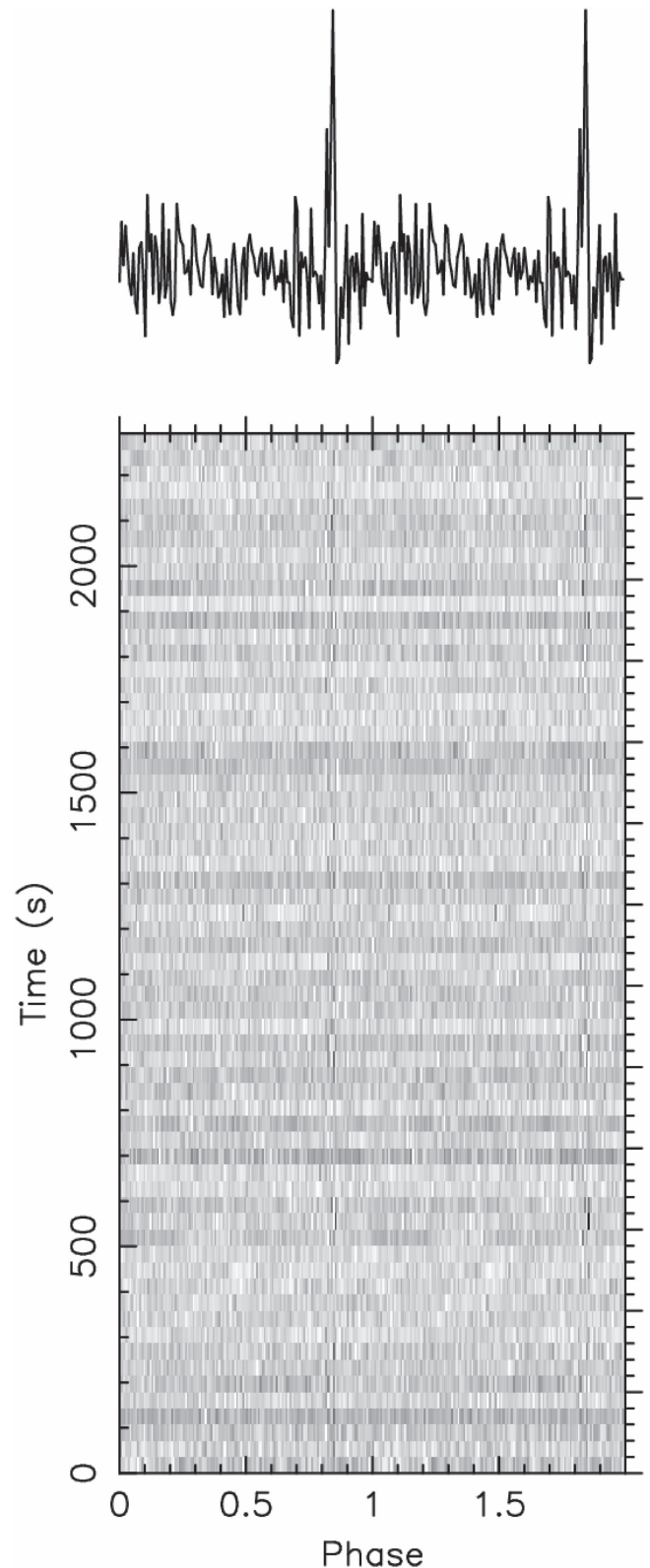


**Figure 1.** Top: the 45 GHz pulse profile of SGR J1745−29 after folding the data for the best-fit period of $P = 3.763504$ s. Bottom: amplitude (grayscale, with darker gray indicating a higher amplitude) as a function of pulsar phase and time during this observation.

VEGAS), roughly ∼2% of the pulse period (Figure 1). This is considerably different from the integrated pulse profile detected at 8.5 GHz before (e.g., Lynch et al. 2015) and after (e.g.,
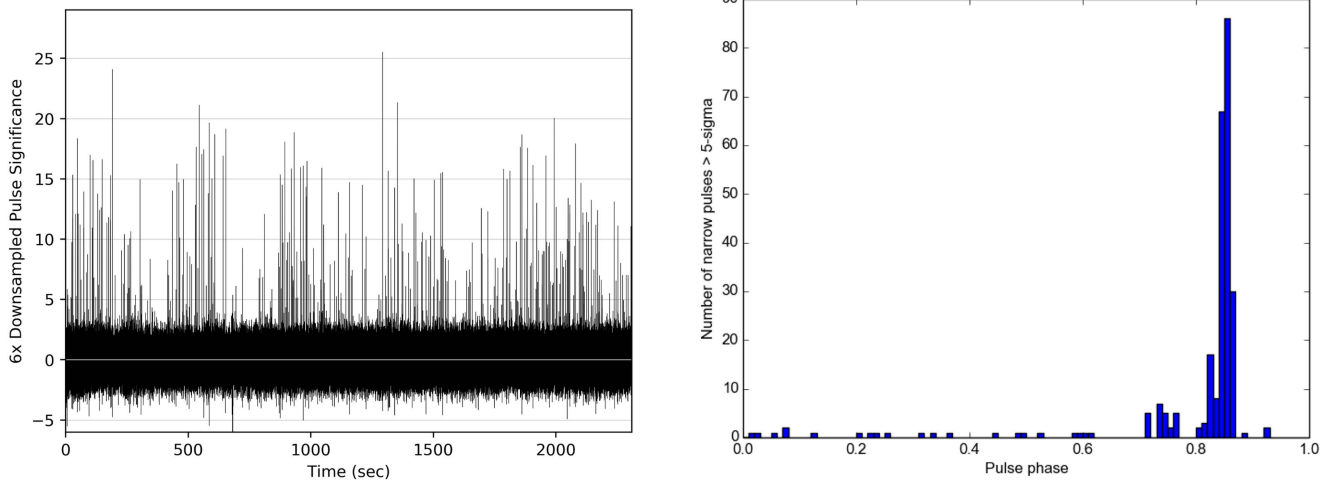
**Figure 2.** Left: significance of pulses detected over a 6 ms time period (the average length of the single pulses discussed in the text) during the 45 GHz GBT observation described in Section 2. This time period is 6× the 1 ms time resolution of VEGAS and is equivalent to downsampling the recorded data 6×. Right: pulse phase resulting from folding the arrival times of samples with S/N > 5 with the observed period of the magnetar.

Torne et al. 2015; Yan et al. 2015) this GBT observation, but comparable to that measured at higher frequencies ($\gtrsim$87 GHz) in the following months (e.g., Torne et al. 2015). The similarity between the widths of the 45 GHz pulse and the "third" component in the 8.7 GHz pulse profile that appeared in 2014 January—March (Lynch et al. 2015) suggests the two are possibly related. Unfortunately, the lack of absolute phase information prevents us from making a stronger connection between these two features.

Since, at this frequency and LST (local sidereal time), no test pulsar suitable for flux calibration was observable, we estimated the pulsed flux density using the pulsar radiometer equation (Appendix A1.4 in Lorimer & Kramer 2012). For the values of $T_{\rm sys}$, $\tau_{\rm zenith}$, and airmass given above and the known GBT $Q$-band gain of 0.68 K/Jy, we derive an average pulsed flux density of $\sim$100 $\mu$Jy. This value corresponds to the average fluence of a single pulse distributed over the magnetar's entire rotation period, with the pulsed emission from this magnetar having a much higher peak brightness.

Furthermore, we found $\gtrsim$430 time bins where the measured signal-to-noise ratio was >5, a significantly higher number than expected assuming Gaussian noise. Their intensity suggests that they are radio frequency interference (RFI) or short bursts of radio emission as observed from other magnetars (e.g., Camilo et al. 2007b). Typically, one would distinguish these two possibilities by looking for dispersion—the change in the arrival time of photons with different frequencies due to their propagation through an intervening plasma. Since RFI is generated locally (either on the Earth's surface or by orbiting satellites), such signals typically are not dispersed, while pulsed emission from astronomical objects is. Unfortunately, despite the very large dispersion measure (DM) toward SGR J1745 $-29$ (DM = 1650 $\pm$ 50 cm$^{-3}$ pc; Shannon & Johnston 2013), this effect is immeasurably small at 45 GHz. An additional method for distinguishing between astronomical pulses and RFI is too look for Faraday rotation, the change in polarization angle with frequency, but this also was not possible due to the lack of polarization information recorded by the VEGAS spectrometer.

Instead, we folded the arrival time of these pulses with the magnetar's rotational period. Since RFI is uncorrelated with magnetar activity, it should be evenly distributed across all rotational phases, in contrast to the pulses produced in the magnetosphere. Indeed, after folding, we found that the arrival times of these samples are heavily concentrated between a pulse phase of $\sim$0.8–0.9 (Figure 2), a clear indication that they are emitted by the magnetar. These pulses had an average width of $\sim$4.62 ms ($\sim$0.1% of the rotational period), comparable to similar pulses observed from other magnetars (e.g, Camilo et al. 2007c; Levin et al. 2012) and considerably shorter than the $\sim$75 ms width ($\sim$2% of the rotational period) of the average pulse. However, the similarity between the average pulse profile (Figure 1) and the phase distribution of the bright radio pulses (Figure 2) suggests that the "average" pulsed radio emission from this magnetar may be a collection of single, bright pulses that vary in pulse phase and intensity—similar to what is believed to occur in other magnetars (e.g., Levin et al. 2012) and the Crab pulsar at low radio frequencies (e.g., Karuppusamy et al. 2010 and references therein). In fact, these single bright pulses dominate the fluence from the pulsar, and together they account for the measured pulse flux density and duration derived from the timing analysis above. This suggests that the pulsed radio emission from the magnetar is dominated by the sporadic generation of bright, short bursts.

Thanks to the multitude of single 45 GHz pulses detected during this GBT observation, we can compare their properties with those detected from this magnetar at $\sim$8.5 GHz. First, the detection of 434 bright ($>5\sigma$) pulses during our GBT observation, which only lasted $\sim$610 pulse periods, implies that this magnetar produced such pulses in $\sim$70% of neutron star rotations. This fraction is significantly higher than the $\sim$3% (53 out of 1913) derived from 8.7 GHz observations several months later (between 2014 June–October; Yan et al. 2015). This discrepancy is unlikely to result from using a different criterion to select "bright" pulses since applying the criterion used by Yan et al. (2015)—peak fluxes >10× the peak flux of the integrated pulse profile—results in a nearly identical collection of pulses. This large difference suggests that either bright pulses are more common at higher frequencies or the rate of bright pulses can vary significantly with time.

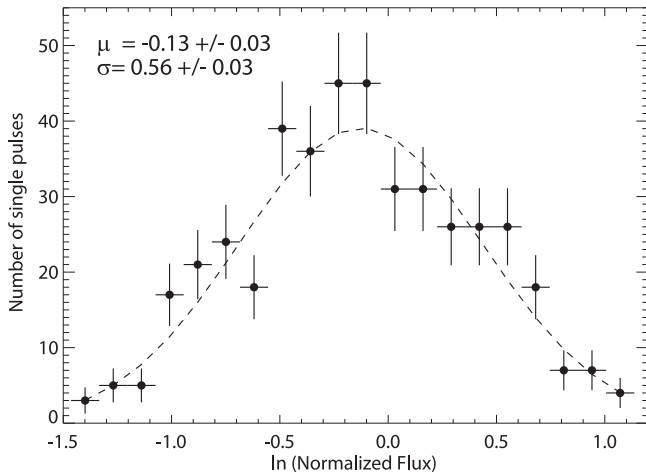We also compared the flux distribution of these 45 GHz single pulses to that detected at 8.7/8.6 GHz from this

**Figure 3.** Normalized flux distribution of 45 GHz single pulses detected from SGR 1745−29, overlaid with the best-fit log-normal distribution as defined in Equation (1). The $1\sigma$ error bars correspond to the square root of the number of single pulses in each log-normalized flux bin.

magnetar (Lynch et al. 2015; Yan et al. 2015). Unlike "normal" radio pulsars, for which the flux distribution of giant pulses is well-described by a power law (e.g., Karuppusamy et al. 2010), the peak flux of single bright pulses from magnetars, like that of "regular" pulses from "normal" radio pulsars (e.g., Burke-Spolaor et al. 2012), is consistent with a log-normal distribution (e.g., Levin et al. 2012),

$$N(x_{\min} < x < x_{\max}) = Ce^{-\frac{(x-\mu)^2}{2\sigma^2}}, \qquad (1)$$

where $x = \ln\left(\frac{S_\nu}{\langle S_\nu \rangle}\right)$, $S_\nu$ is the peak flux density of an individual single pulse, and $\langle S_\nu \rangle$ is the average peak flux density of all single pulses ($\langle S_\nu \rangle = 641$ mJy for the 45 GHz single pulses detected in our GBT observation). As shown in Figure 3, this function (Equation (1)) reproduces the measured distribution of peak flux densities for $\mu = -0.13 \pm 0.03$ and $\sigma = 0.56 \pm 0.03$. This value of $\sigma$ is similar to that measured at 8.6/8.7 GHz both before ($\sigma = 0.49$; Lynch et al. 2015) and after ($\sigma = 0.57 \pm 0.02$; Yan et al. 2015) our GBT observation, possibly suggesting a common generation mechanism.

### 3. Jansky Very Large Array

SGR J1745−29 was serendipitously observed by the JVLA in its A and B configurations as part of NRAO's recent service monitoring campaign of Sgr A$^\star$ (project code TOBS00006; Chandler & Sjouwerman 2013a, 2013b, 2014a, 2014b). During these observations, the WIDAR correlator was configured to achieve a 2 GHz bandwidth centered at 41 GHz. In the analysis described below, we used the calibrated measurement sets available on the NRAO Archive, where flux densities were calibrated using short observations of 3C 286, and the bandpass was calibrated using short observations of NRAO 530 and 3C 286. At 41 GHz, Sgr A$^\star$ (and SGR J1745−29) were only observed for ∼6 minutes on source, and the phases were determined by self-calibrating on Sgr A$^\star$ in the center of the field.[11]

---
[11] See https://science.nrao.edu/science/science-observing for additional details.

The radio environment around Sgr A$^\star$ is extremely complicated; it includes multiple diffuse radio sources that are most likely H II regions and stellar wind bubbles powered by the numerous massive stars in this region (e.g., Zhao & Goss 1998). To minimize the impact of this diffuse emission on our measurements of SGR J1745−29, we only used baselines >500 kλ (>4.8 km) in length to produce our radio images of this field, effectively removing all sources >0″4 in size. We first imaged the remaining data using the CASA task clean, weighting the visibilities on different $u-v$ baselines using the "Briggs" function (Briggs 1995) with a "robust" parameter of 0.5. The resultant image was then deconvolved using the CASA task clean, with "CLEAN boxes" being interactively placed around Sgr A$^\star$, the magnetar SGR J1745−29, and any other sources of emission that appeared after each deconvolution cycle. We measured the flux density of SGR 1745−29 using the MIRIAD (Sault et al. 1995) task imfit to fit a point source at the magnetar's location in the >500 kλ image. The presence of the much brighter Sgr A$^\star$ prevented us from measuring the magnetar's flux density by modeling the measured $u-v$ visibilities with a point source at its location.

As shown in Table 1, eliminating data from shorter baselines generally increased the significance of the magnetar's detection. The flux densities estimated using the method described above typically have substantially larger error bars than those previously reported by Yusef-Zadeh et al. (2015). Using the larger error bars obtained from our analysis, we find values that are in general consistent with, but lower than, those obtained by those authors. The main difference between our two analyses is that Yusef-Zadeh et al. (2015) do not filter out the shorter baselines and modeled the emission from SGR J1745−29 with a 2D Gaussian in the image plane (Yusef-Zadeh et al. 2015). Both differences increase the possible contamination from unrelated diffuse emission around this source and explain why these authors measure a higher, more precise flux density for SGR 1745−29.

We also analyzed an additional JVLA observation of this field taken on 2014 May 10 (Project AG941), which observed SGR J1745−29 for ∼90 minutes with the WIDAR correlator in 8 bit mode in order to achieve the maximum ∼2 GHz bandwidth centered at 44 GHz; this is slightly different from the 41 GHz JVLA observations described above and the 45 GHz GBT observation discussed in Section 2. These data were analyzed using CASA v4.3.1 (McMullin et al. 2007), with the flux density scale, antenna delays, gains, and bandpass all calibrated using observations of 3C 286, while the phases were determined using self-calibration since Sgr A$^\star$ was in the field again. The data were also imaged using the CASA task clean for a "Briggs" weighting (Briggs 1995) of the different $u-v$ baselines with a "robust" parameter of 0.5. The resultant image was then deconvolved, again using the CASA task clean, with "CLEAN boxes" being interactively placed around Sgr A$^\star$, the magnetar SGR J1745−29, and any other sources of emission revealed by further deconvolution cycles. The flux densities of both Sgr A$^\star$ and SGR J1745−29 were then determined by fitting the resultant image with a point at their locations using the MIRIAD task imfit. Sgr A$^\star$ has a 44 GHz flux density of 1.59 Jy in data collected on all baselines as well as in data collected only in baselines >500 kλ in length, consistent with other measurements around this date (Yusef-Zadeh et al. 2015).

We searched for changes in the magnetar's flux density during this observation by dividing this data set into ∼20 minute
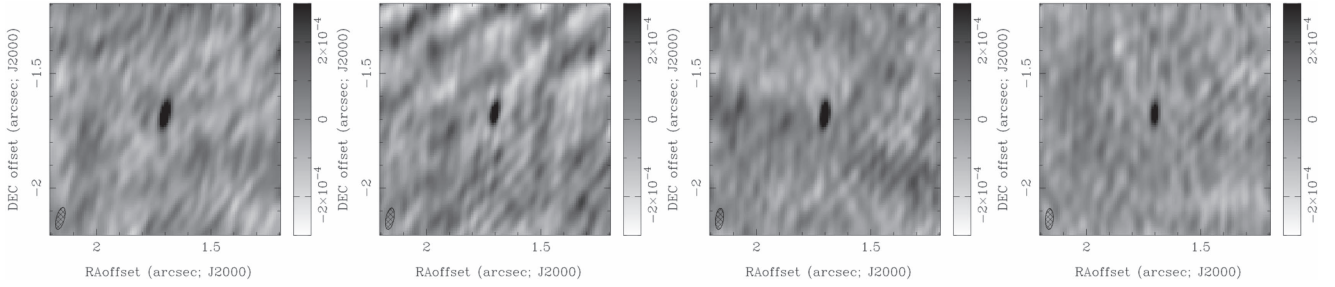
**Figure 4.** 44 GHz images centered on the position of SGR J1745−29 produced using data from the four time periods listed in Table 2. In each image, the grayscale ranges from −0.3 mJy beam$^{-1}$ to 0.3 mJy beam$^{-1}$, and the size and orientation of the resolving beam are shown in the bottom-left corner.

**Table 1**
Compilation of Measured Values of the 41 GHz Flux Density of SGR J1745−29 between 2013 October and 2014 May
(the Reported Flux Density on 2014 May 10 is Actually at 44 GHz)

| Obs. Date YYYY MM DD | JVLA Config. | SGR J1745−29 41 GHz Flux Density (mJy) | | |
|---|---|---|---|---|
| | | >500 kλ | All Data | Yusef-Zadeh et al. (2015) |
| 2013 Oct 26 | B | 2.0 ± 1.0 | 0.50 ± 0.36 | <0.82 |
| 2013 Nov 29 | B | 1.0 ± 0.6 | 0.83 ± 0.46 | <0.7 |
| 2013 Dec 29 | B | 1.2 ± 0.7 | 1.2 ± 1.5 | <1.52 |
| 2014 Feb 15 | A | 2.1 ± 0.4 | 1.6 ± 0.3 | 1.85 ± 0.07 |
| *2014 Feb 21* | A | ⋯ | 1.62 ± 0.02 | 1.62 ± 0.04 |
| 2014 Mar 22 | A | 2.1 ± 0.3 | 0.86 ± 0.22 | 1.24 ± 0.02 |
| 2014 Apr 26 | A | 0.91 ± 0.30 | 0.52 ± 0.25 | 1.20 ± 0.07 |
| 2014 May 10 | A | 1.21 ± 0.22 | 1.10 ± 0.21 | ⋯ |
| 2014 May 31 | A | 3.5 ± 0.4 | 3.5 ± 0.4 | 2.94 ± 0.12 |

**Note.** The reported flux density on 2014 February 21 is taken from Yusef-Zadeh et al. (2014), while the rest were derived using the procedures described in Section 3. The upper limits quoted by Yusef-Zadeh et al. (2015) correspond to the flux density required for a 3σ detection.

**Table 2**
44 GHz Flux Density of SGR 1745−29 and Sgr A* as Measured on 2014 May 10 in mJy

| Source | Time Range (UTC) | | | |
|---|---|---|---|---|
| | 08:23:00−08:41:30 | 08:41:30−09:03:00 | 09:05:00−09:24:00 | 09:24:00−09:43:00 |
| SGR J1745−29 | 1.99 ± 0.38 mJy | 0.88 ± 0.47 mJy | 1.31 ± 0.50 mJy | 0.86 ± 0.52 mJy |
| Sgr A* | 1.590 Jy | 1.585 Jy | 1.590 Jy | 1.588 Jy |
| Image rms | 0.52 μJy beam$^{-1}$ | 0.59 μJy beam$^{-1}$ | 0.52 μJy beam$^{-1}$ | 0.50 μJy beam$^{-1}$ |

**Note.** The error on the flux density of Sgr A* in each time period is ∼0.6 mJy.

increments, imaging each time period separately using the same procedure as described above (Figure 4) and again measuring both the flux density of SGR J1745−29 and Sgr A* by fitting the resultant image with a point at its location using the MIRIAD task imfit. As listed in Table 2, the flux density of the magnetar appeared to vary by a factor of ∼2 between successive ∼20 minute periods in this observation. The constant flux density measured for Sgr A* during this observation, as well as the nearly constant noise level in the image (Table 2, as measured by calculating the rms of pixels in a large source-free region near the magnetar using the KARMA tool kvis; Gooch 2011), suggests that this variability is not an artifact of either our calibration or imaging technique.

The large changes in the magnetar's radio flux density on such short timescale allow us to test the suggestion of Yusef-Zadeh et al. (2015) that the observed radio flux is primarily unpulsed emission generated by the interaction between the magnetar's rotation-powered wind and surrounding medium. These authors argue that, if correct, the unpulsed flux density is proportional to the magnetar wind's ram pressure, $P_{ram} = \rho v_{rel}^2$, where $\rho$ is the density of the surrounding medium and $v_{rel}$ is the

speed of the magnetar relative to its surrounding (Yusef-Zadeh et al. 2015). This suggests that the factor of ∼2 change in flux observed during the 2014 May 10 JVLA observation (Table 2) results from a ∼2× change in ambient density and/or a $\sqrt{2}$× change in $v_{rel}$.

The magnetar's measured transverse velocity $v_{tr} \approx$ 240 km s$^{-1}$ (Bower et al. 2015) suggests it only traveled $\gtrsim 3 \times 10^5$ km (0.002 astronomical units; au) in 20 minutes. If the observed decrease in 44 GHz flux resulted from a decrease in ambient density, the magnetar would have had to pass through a region with an extremely steep density gradient of $\nabla \rho = 5 \Delta n_5 \times 10^7$ cm$^{-3}$ au$^{-1}$, where $\Delta n_5 \equiv \Delta n / 10^5$ cm$^{-3}$ (with $n \approx 10^5$ cm$^{-3}$ the typical density cited by Yusef-Zadeh et al. 2015)—a highly unlikely event. Therefore, a sharp decrease in the unpulsed 41 GHz flux would instead come from a decrease in $v_{rel}$. Since the magnetar's observed proper motion direction is opposite that of blueshifted ∼200 km s$^{-1}$ ionized gas in the region (e.g., Zhao et al. 2009), $v_{rel} \gtrsim 500$ km s$^{-1}$, with Yusef-Zadeh et al. (2015) suggesting that $v_{rel} \sim$ 1000 km s$^{-1}$. Therefore, a ∼2× decrease in the observed flux density requires a $v_{rel}$ decrease of ∼700–1500 km s$^{-1}$. Such a

change could be explained if the magnetar exited the stellar wind bubble of a massive OB or Wolf–Rayet star. However, such bubbles are typically much larger than the distance traversed by this magnetar in ~20 minutes.

Furthermore, if the magnetar did experience a sudden change in ambient density of relative velocity $v_{rel}$, the timescale $\Delta t$ over which the observed radio flux density will change is approximately $\Delta t \sim R/v_{rel}$, where $R$ is the radius of the bow shock (assumed to be the size of the radio-emitting region). For the $R \sim 20$ au as estimated by Yusef-Zadeh et al. (2015), this suggests that $\Delta t \sim v_{1000}^{-1}$ months (where $v_{rel} = 1000 \, v_{1000} \, \mathrm{km \, s^{-1}}$), which is considerably larger than the ~20 minute timescale measured here. Even if changes in the radio emission somehow occurred faster than this estimate, the ~170 minutes it would take light to traverse this ~20 au source makes it nearly impossible for its radio emission to change by a factor of ~2 in only 20 minutes. As a result, we conclude that the high-frequency flux density of SGR J1745−29 is dominated by the magnetar's pulsed emission. In fact, a similar variability on such timescales was observed at higher frequencies ~2–3 months after our JVLA observation on 2014 May 10 (Torne et al. 2015).

However, while both our analysis and that conducted by Yusef-Zadeh et al. (2015) of JVLA observations conducted between 2013 October 26 and 2014 May 31 indicate that while the 41/45 GHz flux density of this magnetar varied significantly during this period (Table 2; ~1–3 mJy), at all epochs the flux density measured by the JVLA was $\gtrsim 5 \times$ –$10\times$ higher than the 45 GHz pulsed flux density of ~0.1 mJy measured by the GBT on 2014 April 10. Since the JVLA observations are sensitive to the total (pulsed and unpulsed) radio emission from the magnetar, while the GBT observation can only measure the magnetar's pulsed radio emission, it may be possible that ~90% of the magnetar's radio emission is unpulsed. However, as described above, the rapid factor of ~2 variability in the magnetar's total (pulsed and unpulsed) radio emission cannot result from changes in its unpulsed radio emission. Therefore, $\gtrsim 50\%$ of the magnetar's total radio emission is pulsed. As a result, together, the GBT and JVLA observations suggest that the magnetar's pulsed high-frequency flux density can vary by almost an order of magnitude. This conclusion is supported by earlier measurements of its pulsed radio measurement—e.g., an extrapolation of the pulsed radio spectrum measured in 2013 May by Shannon & Johnston (2013) suggest a 45 GHz flux density of ~100 $\mu$Jy, comparable to what we measure in our GBT observation (Section 2). Additionally, the 41 GHz flux densities measured in our analysis of service JVLA observations are consistent with the higher frequency pulsed spectrum of the magnetar measured between 2014 July 21 and 2014 August 24 (Torne et al. 2015), again supporting the notion that the magnetar primarily produces pulsed, as opposed to unpulsed, radio emission.

## 4. Summary

To summarize, we present measurements of the ~40 GHz pulsed and total flux density of SGR J1745−29 between 2013 October 26 and 2014 May 31, a period when its 8.5 GHz pulsed radio properties significantly changed (Lynch et al. 2015). Our GBT detection of 45 GHz pulsations on 2014 April 10 (Section 2) is the earliest detection of >20 GHz pulsations from this magnetar, and the narrow, singly peaked profile measured during this epoch is similar to the new component in the 8.5 GHz pulsed profile which appeared a few

months before (Lynch et al. 2015). During this observation, the magnetar emitted a single bright radio pulse in ~70% of its rotations—a significantly higher fraction than previously or subsequently observed at lower frequencies. Furthermore, the peak flux of these bright single 45 GHz pulses follows a log-normal distribution similar to that measured at 8.5 GHz (Figure 3)—another possible connection between the pulsed radio emission at high and low frequencies.

Additionally, our analysis of JVLA observations of SGR J1745−249 during this period (Section 3) suggests its 41 GHz flux density varied by ~5×, consistent with subsequent measurements of its pulsed flux density. The factor of ~2 change in 44 GHz flux density over a ~20 minute period measured during a JVLA observation on 2014 May 10 (Table 2) strengthens the argument for a magnetospheric origin for this high-frequency emission. Although additional observations are needed to test if the connections between the low- and high-frequency pulsed radio emission are real, these results suggest that further study of this magnetar may significantly improve our understanding of the pulsed radio emission from these sources.

## ORCID iDs

Joseph D. Gelfand ⓘ https://orcid.org/0000-0003-4679-1058
Scott Ransom ⓘ https://orcid.org/0000-0001-5799-9714
Chryssa Kouveliotou ⓘ https://orcid.org/0000-0003-1443-593X
Jonathan Granot ⓘ https://orcid.org/0000-0001-8530-8941
Alexander J. van der Horst ⓘ https://orcid.org/0000-0001-9149-6707
Guobao Zhang ⓘ https://orcid.org/0000-0001-8630-5435
Ersin GÖĞÜŞ ⓘ https://orcid.org/0000-0002-5274-6790
Mallory S. E. Roberts ⓘ https://orcid.org/0000-0002-9396-9720
Hend Al Ali ⓘ https://orcid.org/0000-0002-4187-4981

## References

Beloborodov, A. M. 2009, ApJ, 703, 1044
Beloborodov, A. M. 2013, ApJ, 777, 114
Bower, G. C., Deller, A., Demorest, P., et al. 2015, ApJ, 798, 120
Briggs, D. S. 1995, BAAS, 27, 1444
Burke-Spolaor, S., Johnston, S., Bailes, M., et al. 2012, MNRAS, 423, 1351
Bussa, S. & VEGAS Development Team 2012, in American Astronomical Society Meeting Abstracts 219, 446.10
Camilo, F., Ransom, S. M., Halpern, J. P., & Reynolds, J. 2007a, ApJL, 666, L93
Camilo, F., Ransom, S. M., Halpern, J. P., et al. 2006, Natur, 442, 892
Camilo, F., Reynolds, J., Johnston, S., Halpern, J. P., & Ransom, S. M. 2008, ApJ, 679, 681
Camilo, F., Cognard, I., Ransom, S. M., et al. 2007b, ApJ, 663, 497
Camilo, F., Ransom, S. M., Peñalver, J., et al. 2007c, ApJ, 669, 561
Camilo, F., Ransom, S. M., Halpern, J. P., et al. 2016, ApJ, 820, 110
Chandler, C. J., & Sjouwerman, L. O. 2013a, ATel, 5036
Chandler, C. J., & Sjouwerman, L. O. 2013b, ATel, 5545
Chandler, C. J., & Sjouwerman, L. O. 2014a, ATel, 5727
Chandler, C. J., & Sjouwerman, L. O. 2014b, ATel, 5969
DuPlain, R., Ransom, S., Demorest, P., et al. 2008, Proc. SPIE, 7019, 70191D
Gooch, R. 2011, Karma: Visualisation Test-Bed Toolkit, Astrophysics Source Code Library, ascl:1102.018

Ibrahim, A. I., Markwardt, C. B., Swank, J. H., et al. 2004, ApJL, 609, L21
Karuppusamy, R., Stappers, B. W., & van Straten, W. 2010, A&A, 515, A36
Kijak, J., Tarczewski, L., Lewandowski, W., & Melikidze, G. 2013, ApJ, 772, 29
Lazarus, P., Brazier, A., Hessels, J. W. T., et al. 2015, ApJ, 812, 81
Levin, L., Bailes, M., Bates, S., et al. 2010, ApJL, 721, L33
Levin, L., Bailes, M., Bates, S. D., et al. 2012, MNRAS, 422, 2489
Lorimer, D. R., & Kramer, M. 2012, Handbook of Pulsar Astronomy (Cambridge: Cambridge Univ. Press)
Lynch, R. S., Archibald, R. F., Kaspi, V. M., & Scholz, P. 2015, ApJ, 806, 266
Lynch, R. S., Kaspi, V. M., & Scholz, P. 2014, ATel, 6064, 1
McMullin, J. P., Waters, B., Schiebel, D., Young, W., & Golap, K. 2007, in ASP Conf. Ser. 376, Astronomical Data Analysis Software and Systems XVI, ed. R. A. Shaw, F. Hill, & D. J. Bell (San Francisco, CA: ASP), 127
Mori, K., Gotthelf, E. V., Zhang, S., et al. 2013, ApJL, 770, L23
Ransom, S. M. 2001, PhD thesis, Harvard Univ.

Rea, N., Esposito, P., Pons, J. A., et al. 2013, ApJL, 775, L34
Sault, R. J., Teuben, P. J., & Wright, M. C. H. 1995, in ASP Conf. Ser., Vol. 77, Astronomical Data Analysis Software and Systems IV, ed. R. A. Shaw, H. E. Payne, & J. J. E. Hayes (San Francisco, CA: ASP), 433
Serylak, M., Stappers, B. W., Weltevrede, P., et al. 2009, MNRAS, 394, 295
Shannon, R. M., & Johnston, S. 2013, MNRAS, 435, L29
Thompson, C. 2008a, ApJ, 688, 1258
Thompson, C. 2008b, ApJ, 688, 499
Thompson, C., Duncan, R. C., Woods, P. M., et al. 2000, ApJ, 543, 340
Torne, P., Eatough, R. P., Karuppusamy, R., et al. 2015, MNRAS, 451, L50
Yan, Z., Shen, Z.-Q., Wu, X.-J., et al. 2015, ApJ, 814, 5
Yusef-Zadeh, F., Diesing, R., Wardle, M., et al. 2015, ApJL, 811, L35
Yusef-Zadeh, F., Roberts, D., Heinke, C., et al. 2014, ATel, 6041, 1
Zhao, J.-H., & Goss, W. M. 1998, ApJL, 499, L163
Zhao, J.-H., Morris, M. R., Goss, W. M., & An, T. 2009, ApJ, 699, 186